Supporting Information

The Electrochemistry of Sputtered Hematite Photoanodes: A Comparison of Metallic DC versus Reactive RF Sputtering

Rochan Sinha[†], *Reinoud Lavrijsen*[#], *Marcel A. Verheijen*[#], *Erwin Zoethout*[†], *Han Genuit*[†], *Mauritius C. M. van de Sanden*[†,#], *Anja Bieberle-Hütter*[†,*]

[†] Dutch Institute for Fundamental Energy Research (DIFFER), P.O. Box 6336, 5600 HH Eindhoven, the Netherlands

[#] Department of Applied Physics, Eindhoven University of Technology (TU/e), P.O. Box 513, 5600 MB Eindhoven, the Netherlands

KEYWORDS: Hematite, photoelectrochemistry, water splitting, magnetron sputtering, electrochemical impedance spectroscopy.

*Corresponding Author
Email: a.bieberle@differ.nl

Figure S1 (a) shows a top-view SEM image of an uncoated FTO substrate. It has a rough morphology with large grain size distribution (40-300 nm). Figures S1 (b) and (c) show an RF 50 nm thick film on FTO glass before and after annealing, respectively. Before annealing the grain sizes are 40-200 nm and each grain consists of 5-10 nm sized 'nucleates'. These nucleates grow and merge together during annealing and are not observed in the SEM image after annealing. The grains also appear to coarsen during annealing along with the disappearance of smaller grains. Figures S1 (d) and (e) show the low magnification, cross-sectional HAADF-TEM images of the DC and RF thin films after annealing, respectively.

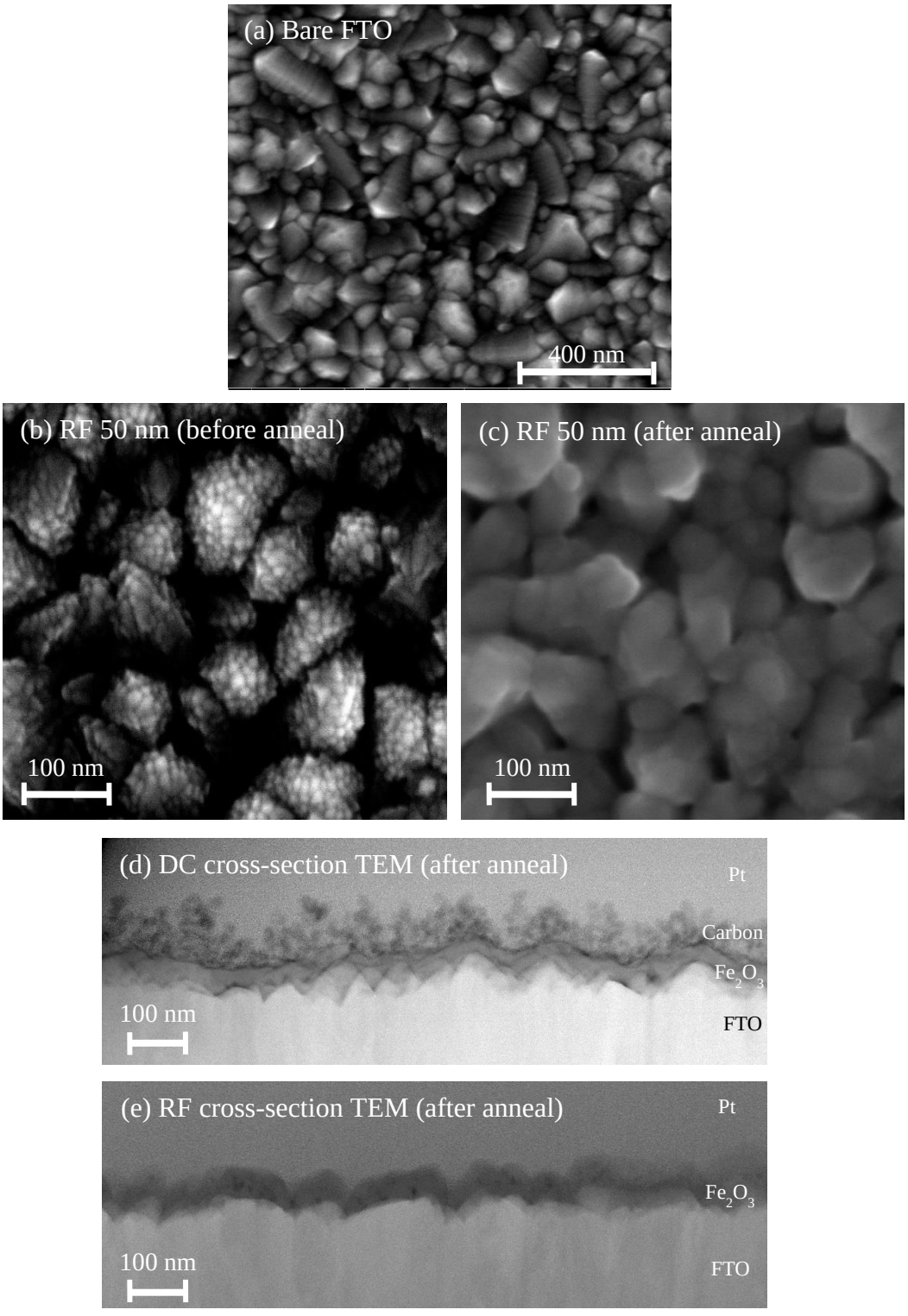

Figure S1. Top-view SEM images of (a) bare FTO substrate and of an RF 50 nm film on FTO glass (b) before annealing and (c) after annealing at 645°C for 10 min in air. Low-magnification cross-sectional TEM image of (d) DC film and (e) RF film after annealing.

Figure S2 shows the GI-XRD spectra of RF sputtered hematite before and after annealing in the 2θ range of 32°-37° in order to display the changes in the peaks corresponding to the (104) and (111) crystal orientation. The peaks shift and increase in intensity during annealing while the peak for the FTO substrate remains unchanged. The peak shift occurs as result of a change in the lattice constants of the hexagonal unit cell of hematite[1]. From the fitting of the hematite peaks, the variation in lattice constants were calculated. The lattice constant 'a' changes from 5.038 Å to 5.025 Å, while the lattice constant 'c' changes from 13.772 Å to 13.716 Å.

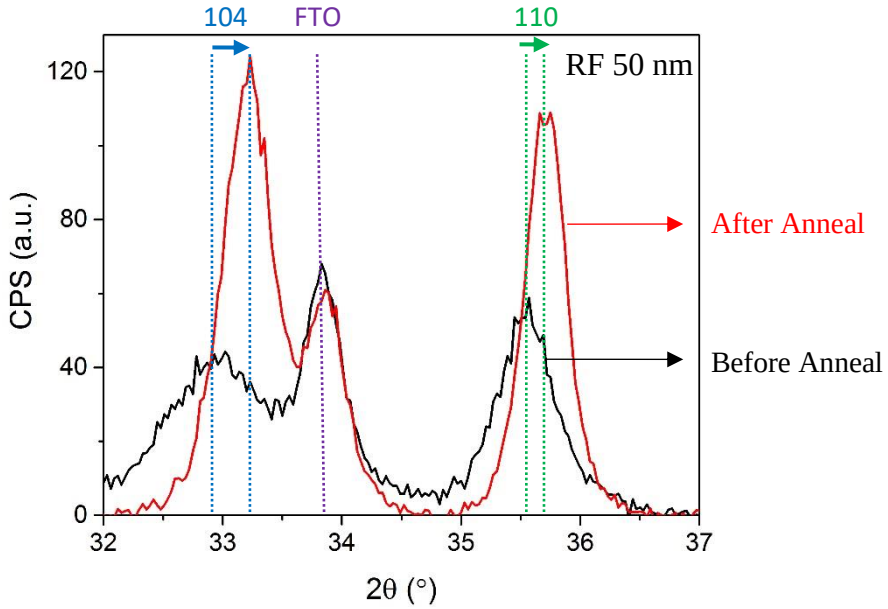

Figure S2. GI-XRD spectra of RF 50 nm film on FTO glass before and after annealing. The shift in peak positions of the (104) peak (blue dotted line) and the (110) peak (green dotted line) are shown by the blue and green arrows, respectively. The FTO substrate peak (purple dotted line) does not shift.

Figure S3 shows the Fe $2p_{3/2}$ spectra for the DC and RF thin films after annealing. The Fe $2p_{3/2}$ peaks are fitted using the XPS spectral parameters for α-Fe_2O_3 as proposed by Biesinger et al.[2] including binding energy position, percentage of total area, full width at half maximum (FWHM) value and spectral component separation. The fit closely represents the Fe $2p_{3/2}$ spectra for both DC and RF films, suggesting that α-Fe_2O_3 is found at the surface of both. However, the fit obtained for the DC film is better than for the RF film, since it has a lower residual value (DC: 1.48 vs. RF: 1.52). The fits for both DC and RF films deviate from the spectra at lower binding energies in the range of 709 eV - 710 eV. This deviation is more pronounced for the RF than for the DC film and is related to the possible presence of other species of iron oxide, such as a hydroxide/oxyhydroxide or a defective oxide at the surface of the film. A fit with multiple iron species is beyond the scope of this article.

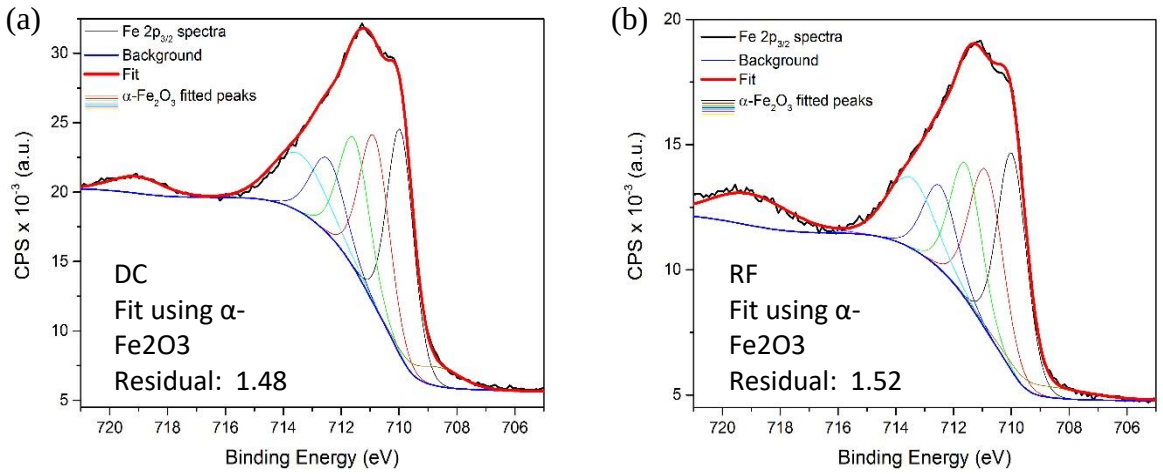

Figure S3. XPS data of the Fe 2p3/2 peak including background and fitting data for (a) DC and (b) RF films.

Figure S4 (a) and (b) show the optical absorption coefficient and Tauc plots of the DC and RF thin films, respectively. The absorption data is corrected for the actual film thickness. A slightly higher absorption coefficient is observed for the DC film in the measured wavelength region compared to the RF film (see main manuscript). The indirect optical bandgap obtained from the Tauc plot is 2.1 eV ± 0.1 eV for both DC and RF films.

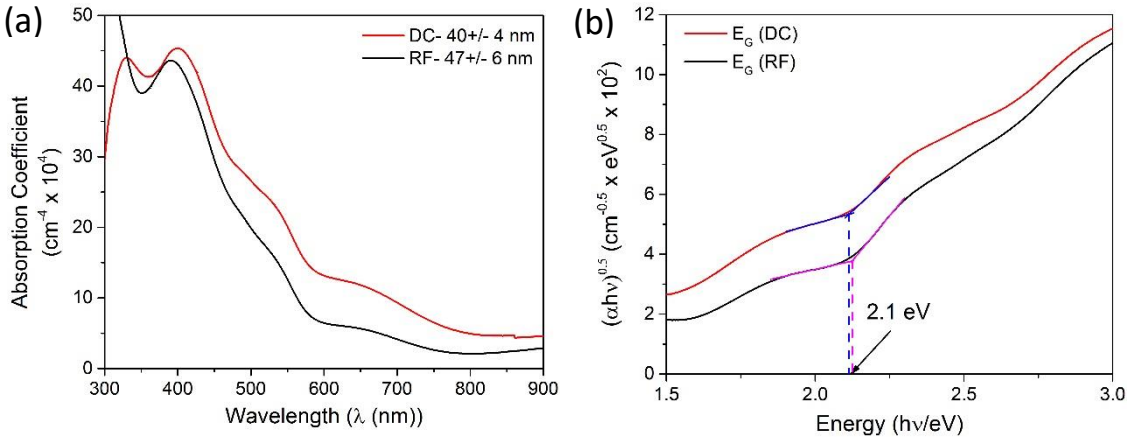

Figure S4. (a) Optical absorption coefficient for DC and RF sputtered thin films annealed at 645°C. The spectra are corrected for the substrate and are obtained by normalising the absorbance with the thickness of the thin films obtained from cross-section TEM images. (b) Tauc plot for the indirect optical bandgap calculation of the DC and the RF thin films.

Figure S5 shows the average values of the onset potentials (V_{onset}) and photocurrent (I) at 1.23 V and 1.5 V versus RHE for all DC and RF films annealed at 645°C and 800°C.

It can be seen that annealing at higher temperatures leads to a decrease in V_{onset} for both DC and RF films which can be attributed to Sn diffusion into the hematite lattice[3]. This shift also leads to higher photocurrent at 1.23 V versus RHE for both DC and RF films. However, the photocurrent at 1.5 V versus RHE is lower for both DC and RF films. This is explained by the ohmic loss due to the increase in FTO resistivity on annealing at 800°C.[3]

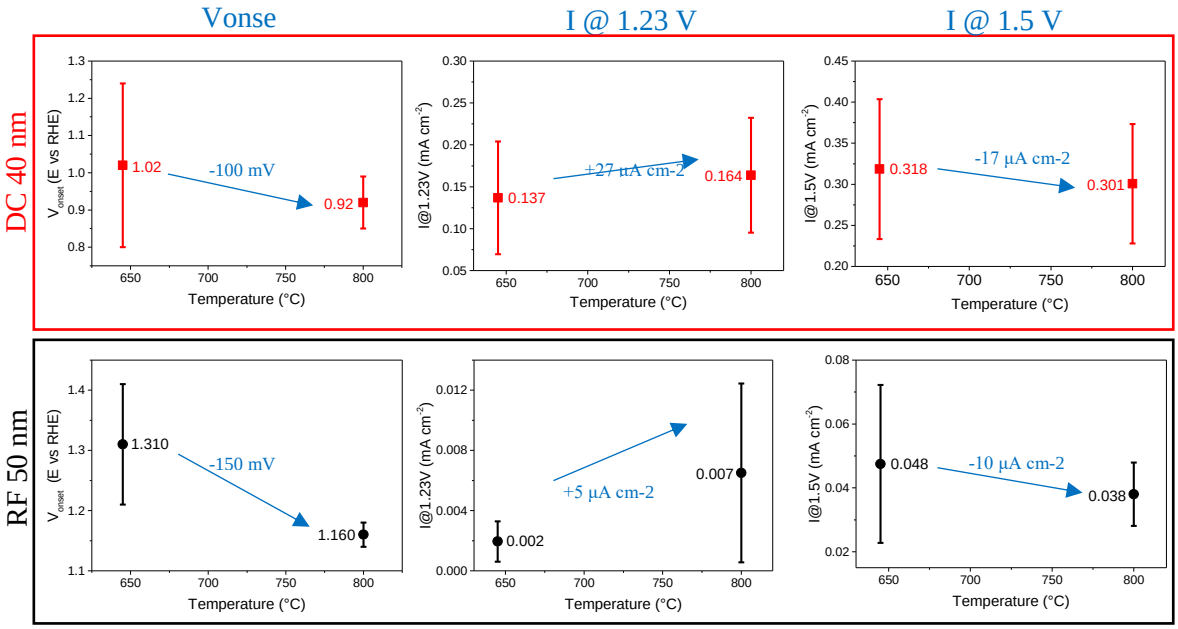

Figure S5. The average values for onset potential (Vonset) and photocurrent at 1.23 VRHE (I@1.23 V) and at 1.5 VRHE (I@1.5 V) for the DC 40 nm and RF 50 nm films. Number of samples measured: DC 40 nm 645°C: 15; DC 40 nm 800°C: 5; RF 50 nm 645°C: 2; RF 50 nm 800°C. All measurements were done in 1M NaOH and under 100 mW cm-2 illumination. Photocurrent values were corrected for dark current at the corresponding potentials (1.23 V and 1.5 V versus RHE).

Figure S6 shows the Nyquist plot of a typical IMPS response for a hematite thin film annealed at 645°C. The low frequency intercept (LFI) representing the steady state photocurrent is represented by a green square. The high frequency intercept (HFI) representing the hole flux is shown by a blue square. The maximum of the semicircle in the upper quadrant of the spectrum gives the ω_{max} value represented as a red square. The larger semicircle in the lower quadrant part of the spectrum represents the RC attenuation circle and the radial frequency at the minimum of this semicircle is given by[4],$\omega_{min} = \frac{C_{SC} + C_H}{R \cdot C_{SC} \cdot C_H}$,where C_{SC} and C_H are the space charge layer capacitance and Helmholtz layer capacitance, respectively, associated with the hematite-electrolyte interface. R is the contact resistance. Provided that the two time constants, ω_{max} and ω_{min}, are separated by at least one order of magnitude, then the upper semicircle can be used to determine values of k_t and k_r.[4] This is the case for the DC and RF films studied in this work.

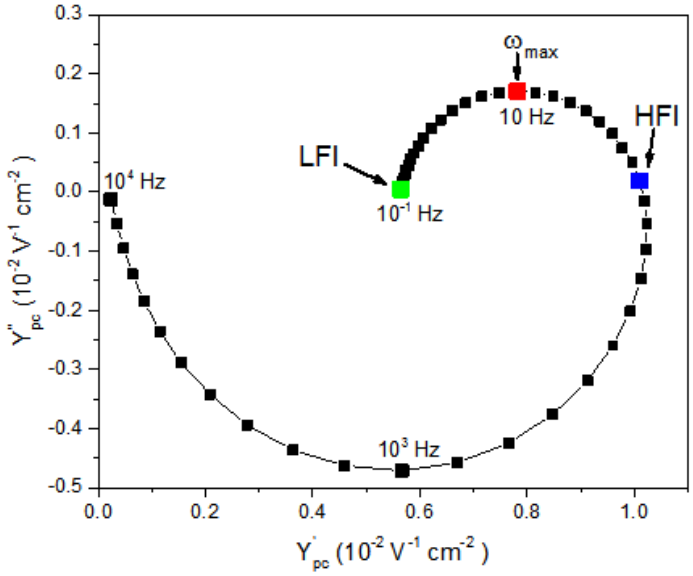

Figure S6. Nyquist plot of the IMPS response for a hematite thin film annealed at 645°C for 10 min. The measurement was done in 1 M NaOH electrolyte under illumination intensity of 22 mW cm-2 at an applied potential of 1 V versus RHE. Low frequency intercept (LFI) and high frequency intercept (HFI) are labelled, respectively.

Table S1 contains the ECM fitting data of the EIS data shown in Fig. 6 in the main manuscript. The ECM was adopted from Klahr et al.[5] and is shown in Figure 6(b) of the main manuscript.

Table S1. ECM fitting data obtained by fitting of the impedance spectra obtained for both the DC and RF films between 0.6 V and 1.6 V versus RHE. Measurements were performed in 1 M NaOH electrolyte under an illumination intensity of 100 mW cm^{-2}.

RF Film

Potential	Chi-Sqr (χ^2)	Rs	CPE_bulk-T	CPE_bulk-P	R_trap	R_ss	CPE_ss-T	CPE_ss-P
0.6	8.39E-04	15.896	1.34E-05	0.825	1303.1	7197.665	3.80E-05	0.754
0.7	6.69E-04	15.786	1.12E-05	0.836	1496.21	11271.81	4.29E-05	0.718
0.8	2.75E-04	16.398	6.75E-06	0.884	783.273	35450.6	5.45E-05	0.552
0.9	2.18E-04	16.563	5.36E-06	0.903	715.92	26774.78	4.47E-05	0.578
1	3.20E-04	16.532	4.86E-06	0.909	828.96	17890.93	3.20E-05	0.644
1.1	6.25E-04	16.634	4.20E-06	0.920	855.65	18807.81	3.03E-05	0.66
1.2	2.65E-04	16.430	4.00E-06	0.920	958.485	25298.19	3.67E-05	0.673
1.3	2.74E-04	16.304	3.92E-06	0.919	1029.92	84261.9	6.11E-05	0.696
1.4	5.37E-04	16.163	3.86E-06	0.918	978.11	38292.3	9.23E-05	0.792
1.5	6.04E-04	16.0768	3.86E-06	0.916	894.115	5083.66	1.24E-04	0.836
1.6	7.78E-04	15.841	4.46E-06	0.902	753.835	1617.1	1.76E-04	0.731
0.6	7.74E-04	16.0376	5.37E-06	0.887	218.779	688.8375	2.57E-04	0.512

DC Film

Potential	Chi-Sqr (χ^2)	Rs	CPE_bulk-T	CPE_bulk-P	R_trap	R_ss	CPE_ss-T	CPE_ss-P
0.6	0.00159	7.781	3.92E-05	0.716	262.033	13345	1.14E-05	0.92755
0.7	5.90E-04	7.459	3.45E-05	0.715	225.609	29906.93	1.44E-05	0.85718
0.8	6.69E-04	7.262	2.92E-05	0.720	210.772	43297.46	1.94E-05	0.85838
0.9	0.0023	6.79	3.60E-05	0.69	263.446	49491.89	5.91E-05	0.83664
1	0.00378	6.215	4.72E-05	0.661	329.778	1033.84	2.15E-04	0.84395
1.1	1.44E-04	7.41	7.70E-06	0.822	102.756	789.71	9.46E-05	0.59705
1.2	2.40E-04	7.341	7.59E-06	0.821	134.470	1485.22	4.44E-05	0.6799
1.3	4.60E-04	7.272	7.80E-06	0.817	167.126	2578.72	2.68E-05	0.7384
1.4	4.44E-04	7.302	6.93E-06	0.827	164.300	3866.91	2.71E-05	0.7269
1.5	0.00118	7.219	7.81E-06	0.815	173.328	5112.71	4.50E-05	0.67399
1.6	0.00246	6.716	1.67E-05	0.747	172.543	2004.11	1.33E-04	0.78467

Figure S7 shows the Mott-Schottky analysis for both DC and RF films in order to estimate the flatband potential (V_{FB}) and donor density (N_D). The analysis was done both in presence and absence of a hole scavenger (Figure S7 (a) and (b), respectively). In both cases, it is observed that there is a difference in the slopes for applied potentials below 1.1 V (low V regime) and above 1.1 V (high V regime). Thus, linear fitting is performed separately for the 2 regimes.

In the high V regime, the curves flatten (pronounced for DC films) leading to unrealistically negative V_{FB} values for both DC and RF films. Thus, for estimating the V_{FB} and N_D values, we consider the low V regime. The estimated flatband potential is 0.3±0.03 V for the DC film; this is comparable to the literature[6]. It also relates well to the onset potential for the PEC measurement with hole scavenger (Figure 8), with photocurrent observed for the entire potential window.

For the RF film, a flatband potential of -0.34V is obtained; this seems unrealistic since it would lie more negative than the conduction band of hematite[7]. Furthermore, from the hole scavenger PEC measurements as shown in Figure 8, we see that the photocurrent drops almost to zero at a potential of 0.65 V. Since the use of a hole scavenger suggests that the overpotential for water oxidation should be negligible, the onset potential should approximately correspond to the flatband potential. This would suggest that the actual flatband potential for the RF film lies in the range of 0.65 V and thus, the value obtained from the Mott-Schottky analysis is underestimated. The unrealistic low flatband potential might be related to various possible reasons, such as fermi level pinning by surface states, difference in relative adsorption of charge species on surfaces with difference in crystalline orientation and chemical composition, or non-planar electrode surface.[7]

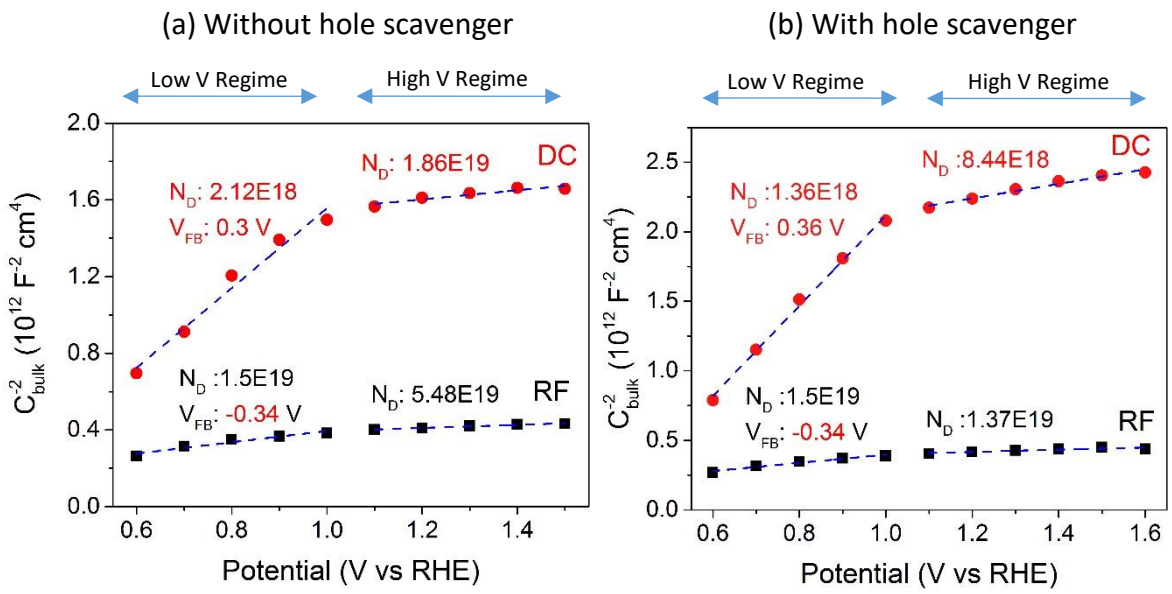

Figure S7 Mott-Schottky plots for DC and RF films measured in (a) 1M NaOH (without hole scavenger) and (b) 1M NaOH + 0.1 M H_2O_2 (with hole scavenger) in the potential range of 0.6 V to 1.6 V versus RHE. Applied potential less than 1.1 V is referred to as the 'Low V regime' while potentials above 1.1 V are referred to as 'High V regime'. The blue dotted lines are the linear fits performed for the M-S curves for both DC and RF films. A change in slope is observed on going from the 'low V regime' to the 'High V regime' which is the reason for separate linear fits performed for the 2 regions. N_D denotes the donor density and V_{FB} denotes the flatband potential.

Figure S8 shows the hole scavenger measurements for the DC and RF films annealed at 800°C. The photocurrent for the DC films is higher than that of the RF film in the entire potential window; this finding is similar to the 645°C annealed samples (Figure 8).

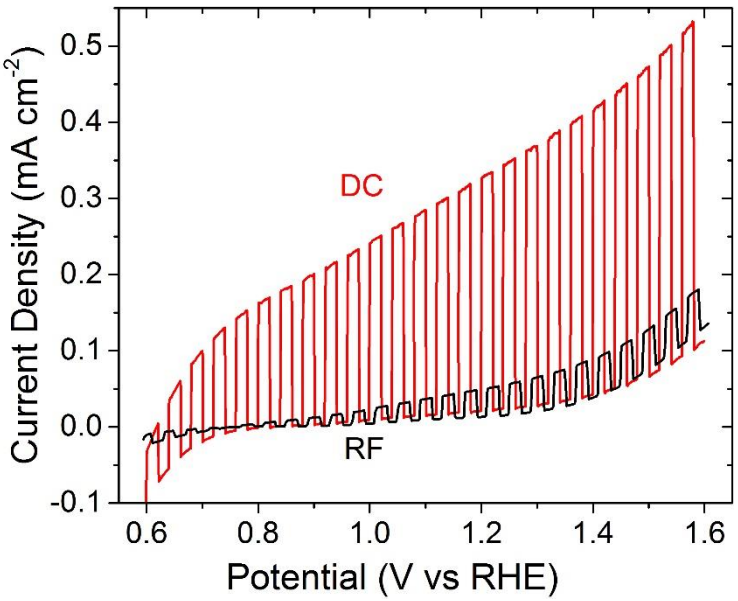

Figure S8 Chopped light measurements performed for the DC (red) and RF (black) thin films (annealed at 800°C) in 1M NaOH + 0.1M H_2O_2 electrolyte. The light was chopped with a frequency of 0.5 Hz. The illumination intensity was 100 mW cm^{-2}.

REFERENCES

(1) Wyckoff, R. W. G. *Crystal Structures*, 2nd ed.; Interscience Publishers: New York, 1963.

(2) Biesinger, M. C.; Payne, B. P.; Grosvenor, A. P.; Lau, L. W. M.; Gerson, A. R.; Smart, R. S. C. Resolving Surface Chemical States in XPS Analysis of First Row Transition Metals, Oxides and Hydroxides: Cr, Mn, Fe, Co and Ni. *Appl. Surf. Sci.* **2011**, *257* (7), 2717–2730.

(3) Annamalai, A.; Subramanian, A.; Kang, U.; Park, H.; Choi, S. H.; Jang, J. S. Activation of Hematite Photoanodes for Solar Water Splitting: Effect of FTO Deformation. *J. Phys. Chem. C* **2015**, *119* (7), 3810–3817.

(4) Peter, L. M. Energetics and Kinetics of Light-Driven Oxygen Evolution at Semiconductor Electrodes: The Example of Hematite. *J. Solid State Electrochem.* **2013**, *17* (2), 315–326.

(5) Klahr, B.; Gimenez, S.; Fabregat-Santiago, F.; Hamann, T.; Bisquert, J. Water Oxidation at Hematite Photoelectrodes: The Role of Surface States. *J. Am. Chem. Soc.* **2012**, *134* (9), 4294–4302.

(6) Khan, S. U. M.; Akikusa, J. Photoelectrochemical Splitting of Water at Nanocrystalline n-Fe_2O_3 Thin-Film Electrodes. *J. Phys. Chem. B* **1999**, *103* (34), 7184–7189.

(7) Hankin, A.; Alexander, J. C.; Kelsall, G. H. Constraints to the Flat Band Potential of Hematite Photo-Electrodes. *Phys Chem Chem Phys* **2014**, *16* (30), 16176–16186.